Research Square

Preprints are preliminary reports that have not undergone peer review.
They should not be considered conclusive, used to inform clinical practice,
or referenced by the media as validated information.

Syntrophic interdependence of microbial activities in photogranules during a feast famine transition

Oriane Della-Negra

oriane.della-negra@inrae.fr

INRAE, Univ. Montpellier, LBE, 102 Avenue des étangs, F-11100

Claire Hoede

Univ Toulouse, INRAE, UR 875 MIAT

Marie-Ange Teste

TBI, Université de Toulouse, CNRS, INRAE, INSA

Christophe Klopp

Univ Toulouse, INRAE, UR 875 MIAT

Rémi Servien

INRAE, Univ. Montpellier, LBE, 102 Avenue des étangs, F-11100

Jérôme Hamelin

INRAE, Univ. Montpellier, LBE, 102 Avenue des étangs, F-11100

Kim Milferstedt

INRAE, Univ. Montpellier, LBE, 102 Avenue des étangs, F-11100

Article

Keywords:

Posted Date: November 25th, 2026

DOI: https://doi.org/10.21203/rs.3.rs-9926149/v1

License: This work is licensed under a Creative Commons Attribution 4.0 International License.
Read Full License

Additional Declarations: No competing interests reported.

Syntrophic interdependence of microbial activities in photogranules during a feast famine transition

O. Della-Negra*, C. Hoede, M.A. Teste, C. Klopp, R. Servien, J. Hamelin* and K. Milferstedt*

Author Information

Affiliations

INRAE, Univ. Montpellier, LBE, 102 Avenue des étangs, F-11100 Narbonne, France

O. Della-Negra, R. Servien, J. Hamelin and K. Milferstedt

Univ Toulouse, INRAE, UR 875 MIAT, Castanet-Tolosan, France

Univ Toulouse, INRAE, BioinfOmics, GenoToul Bioinformatics facility, Castanet-Tolosan, France

C. Hoede and C. Klopp

Univ Toulouse, INRAE, BioinfOmics, Sigenae, Castanet-Tolosan, France

C. Klopp

TBI, Université de Toulouse, CNRS, INRAE, INSA, Toulouse, France

IBISBA-GeT-Biopuces, Toulouse, France

M.A. Teste

Contributions

RS conceptualized and initiated the project. MAT, JH, and KM performed the experiments. CH, MAT, CK, and ODN curated the data. ODN conducted the formal analysis. RS, JH, and KM supervised

the study. ODN wrote the original draft manuscript. All authors contributed to the preparation and revision of the manuscript.

Corresponding author

Correspondence to J. Hamelin (jerome.hamelin@inrae.fr), K. Milferstedt (kim.milferstedt@inrae.fr) and O. Della-Negra (oriane.della-negra@inrae.fr)

Abstract

Oxygenic photogranules contain a phototrophic–heterotrophic consortium of microbes that couples carbon fixation, oxygen production, and pollutant removal, yet the mechanisms underlying their resilience to environmental fluctuations remain unclear. Here, we applied longitudinal metatranscriptomics to investigate how changes in light and carbon supply affect community function. Light exposure reorganized intracellular electron fluxes and reshaped activity across taxa without major compositional changes. Carbon addition buffered redox imbalance and redirected carbon partitioning from cross-feeding interactions toward storage metabolism. Notably, the history of carbon supply determined the duration of regulatory responses, including quorum sensing and biofilm formation, and imprinted persistent changes in co-expression networks. After switching off light, carbon history governed distinct metabolic responses, from anabolic maintenance to nutrient scavenging and denitrification. Together, our results identify metabolic memory, linked to the history of carbon supply, as a key driver of functional adaptation, interaction dynamics and community organization in phototroph-heterotroph consortia.

Introduction

Structured microbial aggregates are widespread in both natural and engineered environments, where they drive key ecological functions through tightly coupled interactions. Oxygenic photogranules are one such system and consist of dense, self-aggregating microbial consortia composed of phototrophic microorganisms, including eukaryotic microalgae and cyanobacteria, intertwined with diverse heterotrophic bacteria[1–3]. Embedded within a matrix rich in extracellular polymeric substances (EPS), these aggregates are similar to biofilms in both their structural complexity and their functional heterogeneity. Steep gradients in light, oxygen, nutrients, and redox potential condition the environment within photogranules. The diversity of microenvironments allows the coexistence on small spatial scales of microorganisms with vastly different environmental needs which gives rise to a metabolic specialization[4].

Oxygenic photogranules are able to simultaneously fix CO_2, produce O_2, and remove organic carbon, nitrogen, and phosphate, as required for wastewater treatment. Close spatial proximity between the different groups of microorganisms allows efficient mass transfer and thus promotes syntrophic interactions[2]. Photogranules have therefore emerged as a promising ecological and biotechnological platform for sustainable wastewater treatment[1]. The functionality and stability of photogranules rely on tightly coupled interactions between their phototrophic and heterotrophic members. Although microalgal–bacterial interactions have been described, cyanobacteria are generally believed to act as the main phototrophic architects of photogranules: filamentous cyanobacteria form an EPS-rich structural scaffold, drive oxygenic photosynthesis, and sustain key metabolic exchanges that are essential for granule cohesion and performance[5,1,6–8]. To test this hypothesis, we analyze closely cyanobacteria-bacteria interactions in the light of photogranule organization and function.

Recent work highlighted multiple and complementary interaction mechanisms between heterotrophic bacteria and cyanobacteria. For example, cyanobacteria stimulate the production of EPS through different mechanisms, such as c-di-GMP–mediated signaling, and provide metabolic precursors that heterotrophic partners[7], such as Acidobacteriota and Chloroflexi, exploit to reinforce physical associations and synthesize adhesive polysaccharides[9]. In return, heterotrophs support phototroph growth via vitamin biosynthesis and by recycling complex organic matter, including polysaccharides, glycerol, and fatty acids, thereby sustaining community carbon fluxes[6,7,9]. Additionally, Kong et al., 2025 showed that cyanobacteria-derived H_2 may fuel hydrogenotrophic denitrifiers, adding a further syntrophic dimension to the metabolic coupling structuring photogranules[10]. Environmental and operational conditions, such as fluctuations in light, nutrient availability, or carbon substrate type, modulate the interactions described above, reshaping transcriptional activity, metabolic fluxes, and interspecies interactions within photogranules. Only a limited number of studies have explored these dynamics, even though such variations can substantially alter photogranule cohesion, pollutant removal efficiency, and metabolic functioning. For example, light limitation redirects carbon fluxes from EPS synthesis toward energy-generating pathways[11], whereas carbon-rich phases promote EPS accumulation as a storage strategy that supports heterotrophic partners during subsequent famine periods[6,12]. Compensatory mechanisms, including alternative carbon fixation routes and coordinated shifts in nitrogen assimilation and EPS restructuring[13,14], further illustrate the ability to adjust resource allocation, metabolic pathway, and interspecies exchanges in response to shifts in fluctuating conditions.

While these studies have advanced our understanding of metabolic complementarity within photogranules, they mainly rely on metabolomic or metagenomic approaches that bias observations toward

abundant, stable compounds and dominant taxa. As a result, key metabolites that are rapidly produced and immediately consumed remain largely undetected, as well as the contributions of minority taxa that may play key roles in community structuring. Complementing these approaches with longitudinal (temporal) metatranscriptomics is therefore essential to detect pathway activation and resolve the functional dynamics underlying microbial interactions. However, simultaneously tracking metabolite turnover and gene expression over time requires substantial methodological developments and remains experimentally demanding.

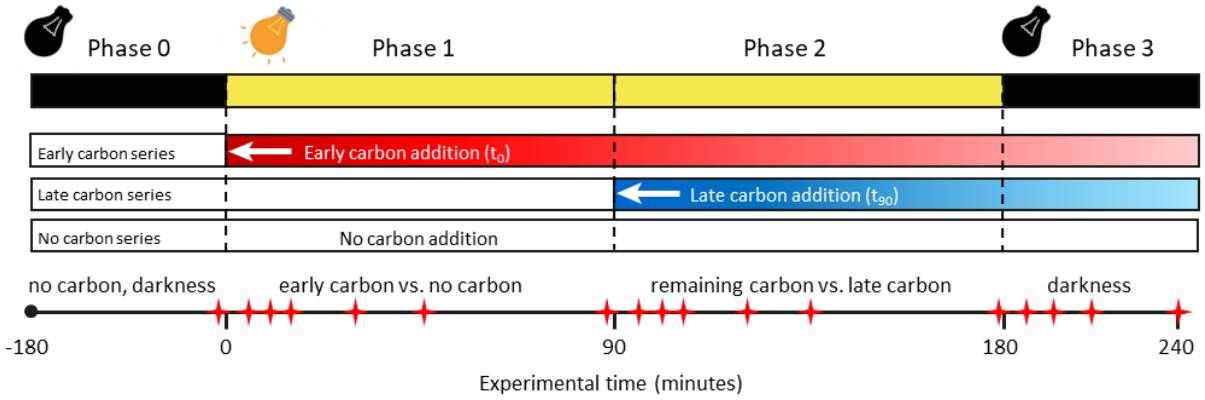
Here, we address this limitation by performing a dynamic, longitudinal metatranscriptomic analysis on the same samples previously characterized by metabolomics[12] using a standardized protocol[15], enabling an integrated interpretation of transcriptional and metabolic responses to controlled environmental transitions. By resolving how cyanobacteria and heterotrophic bacteria adapt their metabolism and interactions under dark/light cycles and feast/famine regimes, this study provides fundamental insights into the mechanisms of interaction that underpin the functional resilience and structural stability of photogranules. Beyond photogranules, the experimental framework and the knowledge gained from this study could be transferable to other phototrophic and syntrophic microbial systems, where robustness results from the tight coupling between metabolic exchanges and regulatory interactions.

Results and discussion

Light and carbon availability drive transcriptional shifts in minority taxa

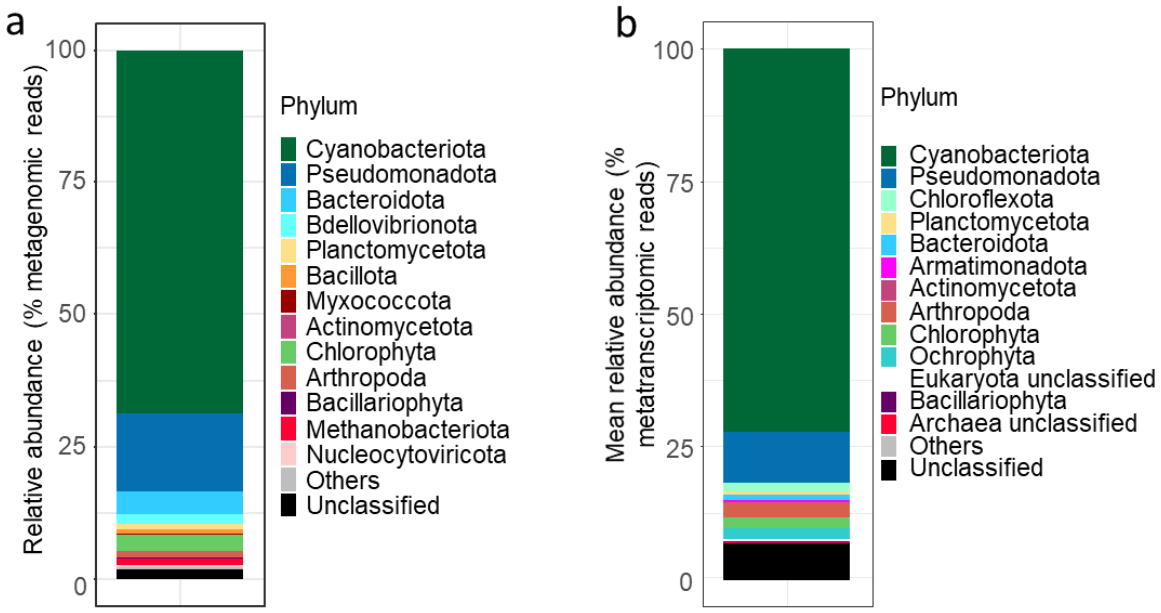
Photogranules were successively exposed to controlled changes of light and nutrient availability, activating either phototrophic microorganisms alone or the entire community, including heterotrophic microorganisms. The three successive light conditions were the following: an initial dark period (Phase 0), followed by two light phases (Phases 1 and 2), and a final dark period (Phase 3, Fig. 1). The nutrient availability conditions corresponded to two experimental series (early carbon series and late carbon series, Fig. 1) that received acetate at different time points (0 and 90 minutes, respectively). The following results, obtained from the analysis of 148 samples, focus on identifying key transcriptomic shifts associated with these changes in light and carbon availability.

Fig. 1: Schematic representation of the experimental phases, indicating the light and the carbon additions. Red crosses represent sampling times.



The microbial community in photogranules was dominated by Cyanobacteriota (~70% of reads) and Pseudomonadota (~10%) in both the metagenome and metatranscriptome, with minor contributions from Bacteroidota, Chloroflexota, and eukaryotic microalgae (Chlorophyta and Ochrophyta, (~2%) (Fig. 2a-b, Fig. S1). Bacteroidota and Bdellovibrionata were the 3rd and 4th most abundant taxa in metagenome. However, considering their abundance, they exhibited an activity that was lower than what could be expected considering their abundance in the metagenome. The analysis of the transcriptome at the genus-level revealed that *Leptolyngbya* was the dominant cyanobacterium and *Thauera* and *Gemnobacter* the main active Pseudomonadota (Fig. S1). These dominant taxa are also commonly found in other photogranules[1]. Slight temporal transcriptome dynamics were observed, with Cyanobacteriota activity increasing during early phases while Pseudomonadota activity decreased in the later phase without light. Microalgal transcription declined following acetate addition (Fig. S2), consistent with potential competition between heterotrophs and phototrophs for organic substrates[16]. Due to their dominance in our system and to focus on bacterial interactions, only contigs from cyanobacteria and heterotrophic bacteria were retained for metatranscriptomic analyses.

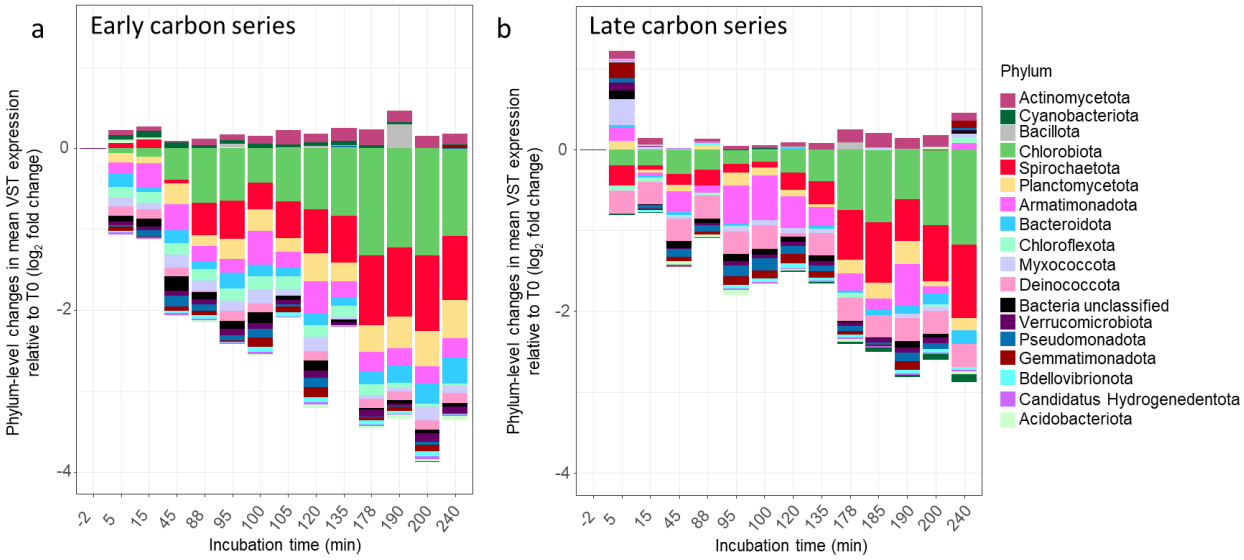
Fig. 2: Community composition of photogranules at T0, at the phylum level in a) the metagenome (% of reads) and b) as an average of n=7 samples in metatranscriptome (% of reads).



The dynamics of changes in mean gene expression at the phylum level revealed patterns uncoupled from taxonomic abundance (**Fig. 3**a-b). Cyanobacteria were nearly absent from this analysis since these taxa were evenly active throughout the duration of the experiment. Light exposure alone induced a downregulation of the activity of Chlorobiota, Spirochaetota, Planctomycetota, Armatimonadota, Bacteroidota, and Deinococcota. In contrast, the combined addition of light and acetate resulted in a broader and stronger downregulation pattern, and was extended to Chloroflexota and Myxococcota (**Fig. 3**a-b, Fig. S3). Overall, the magnitude of transcriptional downregulation was higher in the early carbon series than in the late carbon series, and differences between both series lasted during the experiment (Fig. S3). It suggests that low-abundant taxa (< 2%) are more sensitive to carbon-rich conditions and may be outcompeted or functionally repressed during phases of high resource availability. In our dataset, these minority taxa exhibited mostly negative transcriptional responses (negative log fold changes, **Fig. 3**) rather than strong activation, suggesting that their functional contribution results more from modulation of their activity under competitive or other constraints than from an increase in their transcriptional output[17]. Such dynamics may also play a key role in shaping community-level functional adaptation, consistent with temporal series in microbial consortia, where rare taxa influence functional shifts leading to changes in absolute abundance[18]. Further analysis of temporal dynamics, using metagenomic or metabarcoding approaches, could clarify whether these shifts in abundance occur during light-dark transitions, following acetate addition, or remain stable over time.

Uncoupling metagenomic abundance from changes in activity suggests that minority taxa may contribute disproportionately to transcriptional responses in photogranules, although increased expression may also reflect structural or maintenance-related functions rather than direct metabolic activity. When light was provided, downregulation might reflect redox reorganization driven by photosynthetic oxygen production, reducing the anaerobic volume within the photogranules or polymer-degrading niches, detrimental to anaerobic taxa such as Chlorobiota or Spirochaetota[19,20]. When acetate was added, intensified downregulation across additional phyla likely resulted from rapid competitive takeover by copiotrophic populations, such as dominant Pseudomonadota, which might exploit readily available substrates and nutrients. These dynamics are similar to feast-famine selection observed in activated sludge or aerobic granular sludge systems where carbon addition transiently favors fast-growing heterotrophs while suppressing slower growing, specialized populations[21]. Furthermore, similar stratification and functional redistribution were reported in engineered biofilms, where substrate gradients and oxygen dynamics drive transcriptional shifts without immediate compositional change[22]. The granulation process seems to be driven by dominant taxa[1,21], whereas functional changes and adaptability to environmental conditions appear to be governed by minority taxa. In this context, photogranules appear to behave as light-modulated granular biofilms, where photosynthetic oxygen production and external carbon inputs regulate transcriptional activity, and probably influence trophic interactions across the community, mainly involving minority taxa which may play a role in photogranule adaptability.

Fig. 3: Temporal changes in bacterial activity compared to T0, at the phylum level. Variance-stabilizing transformation (VST) of gene expression was averaged by phylum and transformed to log2 fold change compared to T0 for a) the early carbon series and b) the late carbon series. Δ VST-expression log2FC > 0 indicates activation and < 0 indicates downregulation.



Light-driven redox adaptation and the role of acetate in the modulation of oxidative stress

Enrichment analyses comparing the early carbon series (combined light and carbon effect) and the late carbon series (light effect) in phase 1, relative to phase 0, revealed overlapping and distinct metabolic responses, mainly linked to a shift in intracellular electron fluxes. As indicated in blue, in Fig. 4a (NES score), both series shared a general decrease of the genes expressed in catabolic pathways, that were carried by some Pseudomonadota (*Aquimonas, Thauera, Pseudogemnobacter*, Roseomonadaceae), Bacteroidota (*Phnomibacter*), Chloroflexota (Phototrophicaceae), and Myxococcota (Fig. 4b), indicating an overall reduction in organic carbon oxidation under the effect of light, when photosynthetic activity was initiated. However, the nature of the redox response differed depending on carbon availability.

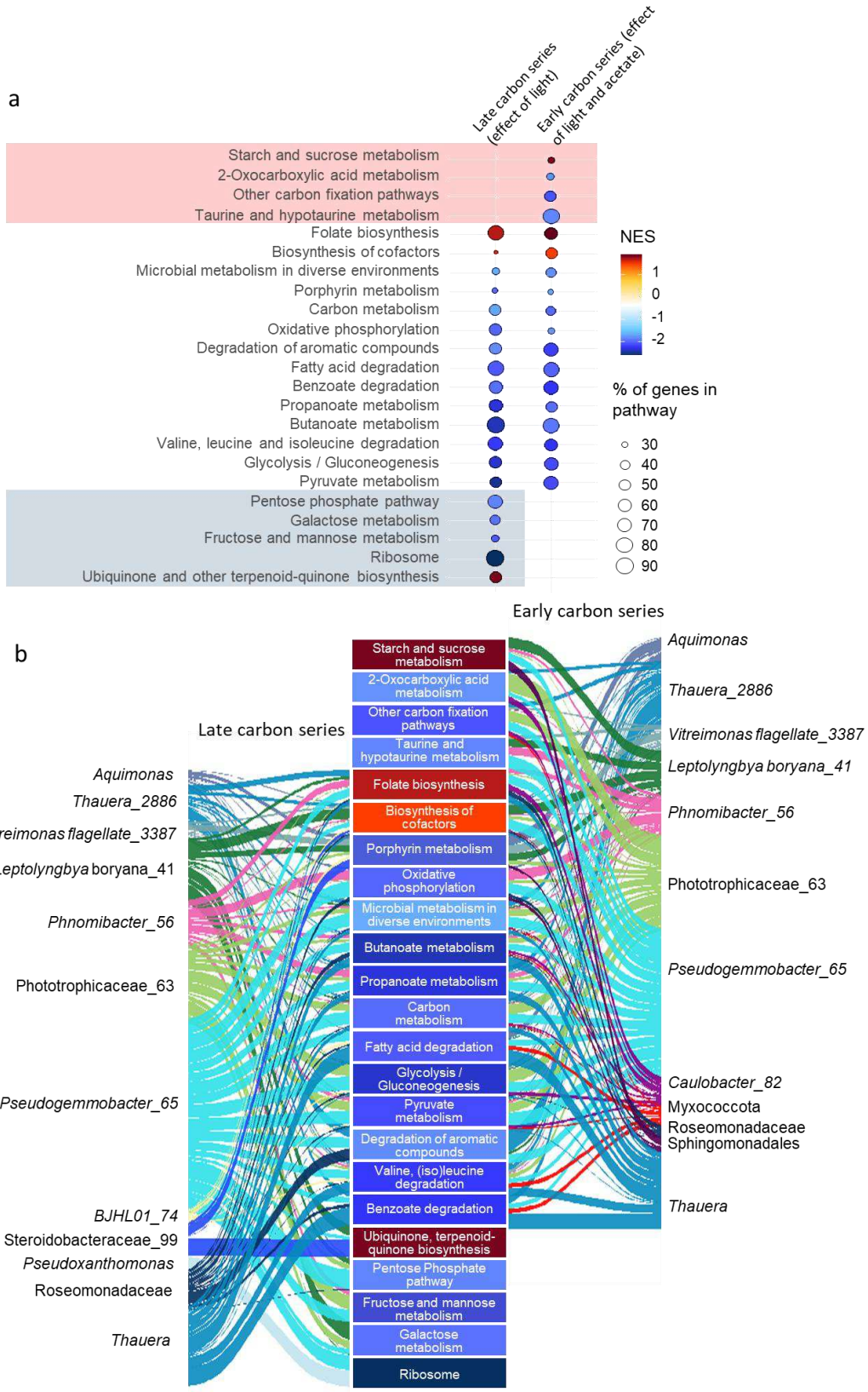
When light became available, phototrophic community members, dominated by Cyanobacteriota (*Leptolyngbya boryana*, Fig. 4b) and Chloroflexota (*Phototrophicaceae),* may redirect energy metabolism toward photosynthetic electron transport and CO_2 fixation, thereby reducing the reliance on organic carbon oxidation as an energy source. Concomitant downregulation of the Pentose Phosphate pathway, sugar metabolism, and ribosomal functions suggests a transient slowdown of heterotrophic and mixotrophic central carbon fluxes and biosynthetic demand (blue rectangle in Fig. 4a, involvements of both heterotrophs and phototrophs in these pathways, Fig. 4b). It also involved a redirection of energy towards folate and cofactor biosynthesis needed for photosynthetic electron transport, carbon fixation, and the production of metabolites required for microbial growth, such as amino acids and nucleotides. Such resource reallocations

were already observed in photogranules[13]. In parallel, the up-regulation of ubiquinone and terpenoid-quinone biosynthesis pathways (Table S1) points to reinforcement of the electron transport chain and expansion of the quinone pool, key components for electron buffering and redox homeostasis. This pattern is consistent with an increased redox pressure generated by oxygenic photosynthesis, which require enhanced capacity for electron dissipation and oxidative stress mitigation[23].

In contrast, when acetate was supplied together with light, quinone-related responses were not observed, and pathways linked to taurine and hypotaurine metabolism were downregulated (red rectangle in Fig. 4a, Table S2). Given the role of hypotaurine as a scavenger of reactive oxygen species [24], and the distinct concentration dynamics between the early and the late carbon series,[12,15] the need for oxidative stress management was reduced when light and carbon were present at the same time. The presence of an external organic substrate might provide an efficient electron sink via heterotrophic respiration, thereby alleviating redox pressure generated by photosynthetic activity.

Taken together, these results indicate that carbon availability determines the response and the adaptation of community members to flux of electrons when light becomes available. Rather than just stimulating biomass production, light influences electron flux within the entire community, increasing intracellular electron pressure and necessitating enhanced scavenging of oxygen radicals[25]. Acetate addition, in turn, redirects electrons toward respiratory pathways, modulating oxidative stress responses. In mixed phototrophic-heterotrophic systems, metabolic stability thus depends on the balance between electron generation through photosynthesis and electron dissipation through respiration or alternative sinks[8]. Carbon addition is therefore not only the growth substrate but also the regulator of community-level redox homeostasis within structured microbial consortia.

Fig. 4: a) KEGG pathways that were significantly enriched in the late carbon series, phase 1 (light effect), or in the early carbon series, phase 1 (combined effect of light and acetate), relative to phase 0. The red rectangle indicates pathways specifically enriched in the early carbon series, whereas the blue rectangle indicates pathways specifically enriched in the late carbon series. b) Sankey diagrams illustrating the contribution of the most influential contributors to the enriched KEGG pathways. Pathways are colored according to their Net Enrichment Score (NES).


a
Late carbon series (effect of light)
Early carbon series (effect of light and acetate)
Starch and sucrose metabolism
2-Oxocarboxylic acid metabolism
Other carbon fixation pathways
Taurine and hypotaurine metabolism
Folate biosynthesis
Biosynthesis of cofactors
Microbial metabolism in diverse environments
Porphyrin metabolism
Carbon metabolism
Oxidative phosphorylation
Degradation of aromatic compounds
Fatty acid degradation
Benzoate degradation
Propanoate metabolism
Butanoate metabolism
Valine, leucine and isoleucine degradation
Glycolysis / Gluconeogenesis
Pyruvate metabolism
Pentose phosphate pathway
Galactose metabolism
Fructose and mannose metabolism
Ribosome
Ubiquinone and other terpenoid-quinone biosynthesis
NES
1
0
-1
-2
% of genes in pathway
30
40
50
60
70
80
90
b
Late carbon series
Early carbon series
Aquimonas
Thauera_2886
Vitreimonas flagellate_3387
Leptolyngbya boryana_41
Phnomibacter_56
Phototrophicaceae_63
Pseudogemmobacter_65
BJHL01_74
Steroidobacteraceae_99
Pseudoxanthomonas
Roseomonadaceae
Thauera
Caulobacter_82
Myxococcota
Roseomonadaceae
Sphingomonadales
Starch and sucrose metabolism
2-Oxocarboxylic acid metabolism
Other carbon fixation pathways
Taurine and hypotaurine metabolism
Folate biosynthesis
Biosynthesis of cofactors
Porphyrin metabolism
Oxidative phosphorylation
Microbial metabolism in diverse environments
Butanoate metabolism
Propanoate metabolism
Carbon metabolism
Fatty acid degradation
Glycolysis / Gluconeogenesis
Pyruvate metabolism
Degradation of aromatic compounds
Valine, (iso)leucine degradation
Benzoate degradation
Ubiquinone, terpenoid-quinone biosynthesis
Pentose Phosphate pathway
Fructose and mannose metabolism
Galactose metabolism
Ribosome

213

Acetate addition increased Chloroflexi-mediated CO_2 fixation and decreases cyanobacterial storage metabolism

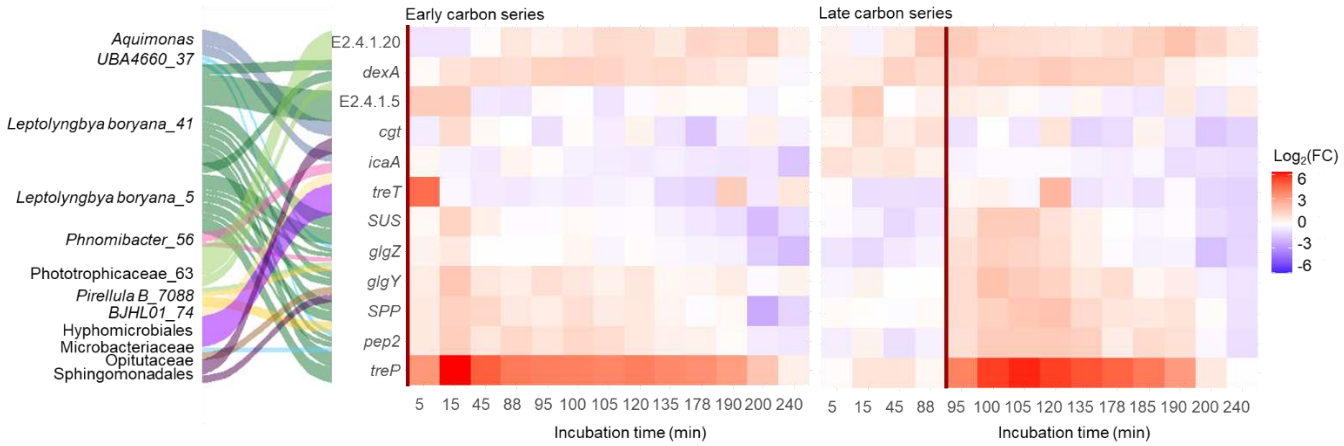
In addition to redox modulation, acetate redistributed carbon fluxes across the microbial consortium. As shown in Fig. 4a (red rectangle), the addition of acetate repressed alternative carbon fixation pathways and 2-oxocarboxylic acid metabolism, associated with a Chloroflexi phototroph (Phototrophicaceae). Some genes involved in CO_2 assimilation into central intermediates (*pycB, aceE, nifJ, bkdA,* and *vorA/vorB,* see Tables S5-S6) were significantly downregulated, indicating a reduced flux from inorganic carbon toward pyruvate, acetyl-CoA, and oxaloacetate (pathways relative to the previous genes). This pattern suggests that under phototrophic conditions, this Chloroflexi, present in the community at < 1%, contributes to CO_2 fixation and its conversion into core metabolic intermediates, consistent with the previous report of 3-hydroxypropionate-based carbon assimilation in Chloroflexi within microbial agregates[14].

In contrast, acetate addition activated starch and sucrose metabolism (including pathways related to carbohydrate interconversion and intracellular storage) with a transcriptional response dominated by *Leptolyngbya boryana.* But several genes activated in this pathway were also found in multiple heterotrophic taxa: Planctomycetes (*Pirellula*, BJHL01), Bacteroidota (UBA4660, *Phnomibacter*), Pseudomonadota (*Aquimonas*, Hyphomicrobiales, Sphingomonadales), and Opitutaceae (Fig. 5). Temporal dynamics, particularly in the late carbon series, revealed successive activation/downregulation phases (Fig. 5), highlighting a strong modulation of carbon metabolism. Prior to acetate addition, phototroph-specific glucosyltransferases (E.C. 2.4.1.20, *dexA*) were expressed, maintaining extracellular polysaccharide (EPS) production. The correlated expression of genes coding for glycosyltransferase and PNAG-poly N-acetylglucosamine synthesis (*cgt, icaA,* Fig. 5, Fig. S4a), carried by *Aquimonas* and *Phnomibacter*, suggested correlated polysaccharide turnover and biofilm structuring. Comparable interactions were reported in phototrophic systems, where heterotrophic bacteria utilize cyanobacterial polysaccharides (from PNAG and alginate EPS-derivatives) while reciprocally providing growth factors, vitamins, and cofactors to cyanobacteria[7]. This pattern was consistent with the persistent expression of *pelE* and *wzy* genes[26] (Fig. S5), both involved in EPS biosynthesis and detected in *Leptolyngbya boryana* across both experimental series. These results support the hypothesis of a cross-feeding regime in which cyanobacterial EPS serve as a carbon source for heterotrophic partners[27], in agreement with previous reports of Bacteroidota and other taxa degrading cyanobacterial polymers[6,9]. Following acetate addition, pathways for EPS synthesis were suppressed, while some genes involved in trehalose and sucrose metabolism (*treP/T, glgY-Z, SUS, SPP,*

Fig. 4a) were activated, mainly in *Leptolyngbya boryana*. These genes encode enzymes linked to intracellular carbohydrate synthesis and storage, indicating a metabolic shift from the accumulation of extracellular carbon toward intracellular carbon accumulation[28].

This metabolic reallocation is consistent with the shift in community-level redox balance, observed previously. Under light alone, photosynthetic electron flow necessitates carbon-consuming outlets such as CO_2 fixation and extracellular polysaccharide production, sustaining cross-feeding interactions. In contrast, acetate assimilation reduces reliance on autotrophic carbon fixation and redirects carbon toward intracellular reserve compounds. The suppression of EPS-related pathways and decreased activation of heterotrophic glycoside-processing genes indicate a transition from an EPS-mediated cross-feeding regime to a storage strategy. Similar shifts were also observed in natural phototrophic systems, where cyanobacteria transitioned from autotrophic growth to the use of dissolved organic carbon or intracellular reserves under low-light or anoxic conditions, involving the activation of EPP, glycolysis, and fermentation pathways[29]. Altogether, it shows a common metabolic response, where both environmental gradients and organic carbon availability drive similar reallocations of carbon fluxes. These results fit within a broader mixotrophic framework, recognized as a prevalent strategy among cyanobacteria. Mixotrophy, the simultaneous use of inorganic and organic carbon, allows for rapid adjustment to changes in environmental conditions[30]. Here, *Leptolyngbya boryana* seems to exhibit a mixotrophic-like behavior; which is complemented by a correlated response of autotrophic and heterotrophic processes at the community level. This functional organization reflects the coupling between metabolic adaptation and community structure in photogranules.

Fig. 5: Temporal dynamics of activated genes (log_2(Fold Change) compared to Phase 0 and belonging to starch and sucrose metabolism in early carbon series and late carbon series. On the left of the heatmaps, the Sankey diagram illustrates the taxa in which genes were present. The vertical brown line indicates acetate addition.



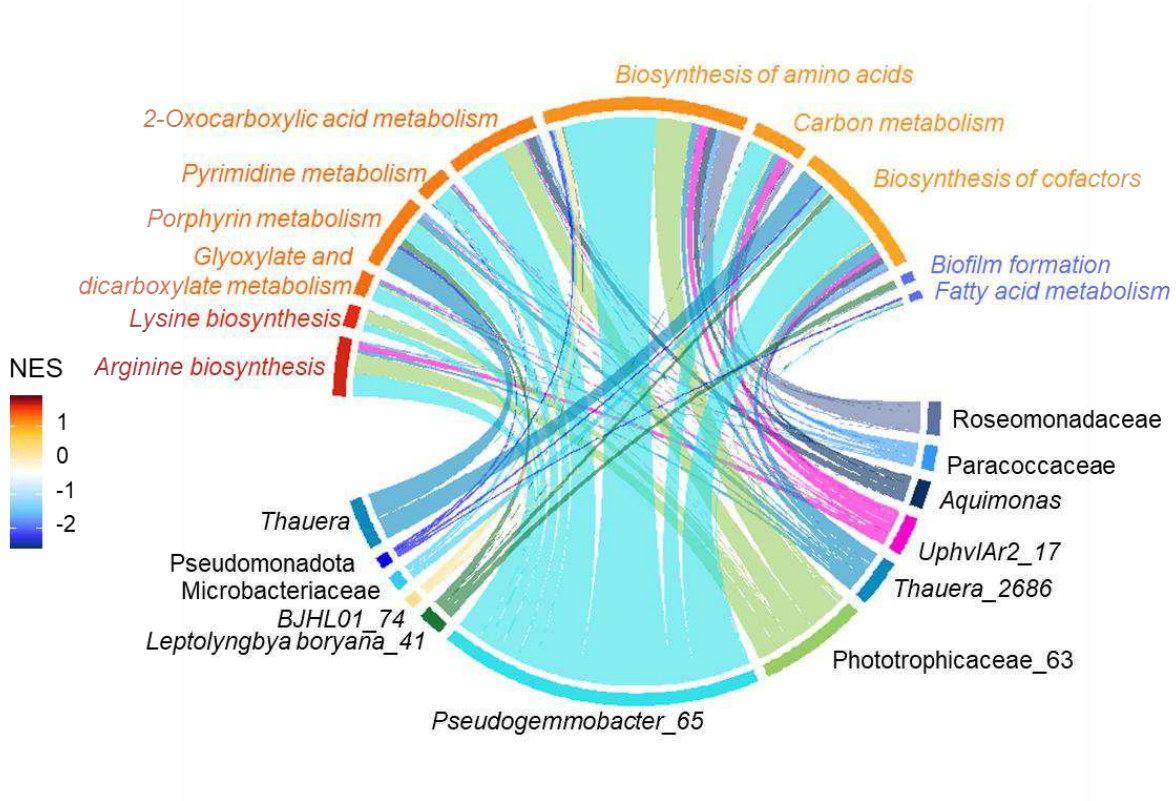
Prolonged exposure to carbon promotes anabolism and reduces storage of lipids

The history of acetate addition relative to light exposure influenced transcriptional profiles (Fig. 6; Table S7). Simultaneous exposure to light and acetate (early carbon series) resulted in stronger enrichment of anabolic pathways compared to acetate addition after 90 minutes of light exposure (late carbon series, Fig. 1), including amino acid biosynthesis (e.g., arginine and lysine pathways), nucleotide biosynthesis (pyrimidine metabolism), cofactor production (porphyrin and other cofactors), and central carbon metabolism (glyoxylate, dicarboxylate, and 2-oxocarboxylic acid pathways, Fig. 6). *Pseudogemnobacter*, was the organism that showed the strongest change in gene expression, indicating a shift from short-term substrate assimilation toward sustained biomass production and cellular maintenance. Higher activity in cofactor and porphyrin metabolism suggests increased demand for redox-active cofactors and enzymatic functions, consistent with an enhanced capacity for redox balancing under simultaneous light and acetate availability, as observed previously. Similar metabolic shifts have been reported in bacterial systems that alternate between biomass growth and nutrient scavenging depending on nutrient availability[31].

In contrast, prolonged acetate availability led to correlated downregulation of fatty acid biosynthesis genes (*ACACA, KAR,* and *TSC13)*. These enzymes catalyze key steps in malonyl-CoA formation and fatty acid chain elongation, and their downregulation indicates reduced flux of acetyl-CoA toward energetically costly lipid production. Instead, acetate-derived carbon appears to be preferentially routed into central metabolism and anabolic processes. This response could reflect a reduced reliance on lipid-associated carbon exchange between phototrophs and heterotrophs under sustained external carbon supply, as observed in other photogranule-like systems[32]. Here, the history of carbon supply modulates the functional role of acetate,

with simultaneous light and acetate availability (early carbon series) promoting its integration into anabolic processes and central carbon metabolism. In contrast, delayed addition after an initial light period (late carbon series) is associated with a reallocation of acetate-derived carbon probably toward maintenance functions.

Fig. 6: KEGG pathways that were significantly enriched in the early carbon series, phase 2 compared to the late carbon series, phase 2 (effect of carbon history). The contributions of the most influential taxa to the enriched KEGG pathways are depicted. Pathways are colored according to their Net Enrichment Score (NES).



Carbon exposure history modulates biofilm regulatory dynamics

The history of carbon exposure influenced biofilm regulation and probably community coordination, via quorum-sensing (Fig. 6). Acetate addition triggered the expression of a number of genes involved in quorum-sensing (*pqsE, rhlB*) and motile-to-sessile transition genes, (*sagS, chpC,* and *wspA*)[33–36] and carried by both heterotrophs and phototrophs (*Pirellula*, *Azonexus, Vitreimonas*, *Leptolyngbya boryana*, *Candidatus Didemnitutus,* and Phototrophicaceae, Fig. 7), followed by sustained activation of the

wsp chemosensory operon[37] (Fig. 7, Fig. S4b). However, the temporal dynamics differed between series. In the early carbon series, light exposure resulted in prolonged activation (45–88 min) of quorum-sensing and motility-regulatory genes, whereas in the late carbon series, activation was shorter (~20 min). Here, the history of carbon exposure modulated the temporal dynamics of microbial regulatory responses, with shorter carbon exposure leading to more transient activation, and longer exposure associated with more sustained responses.

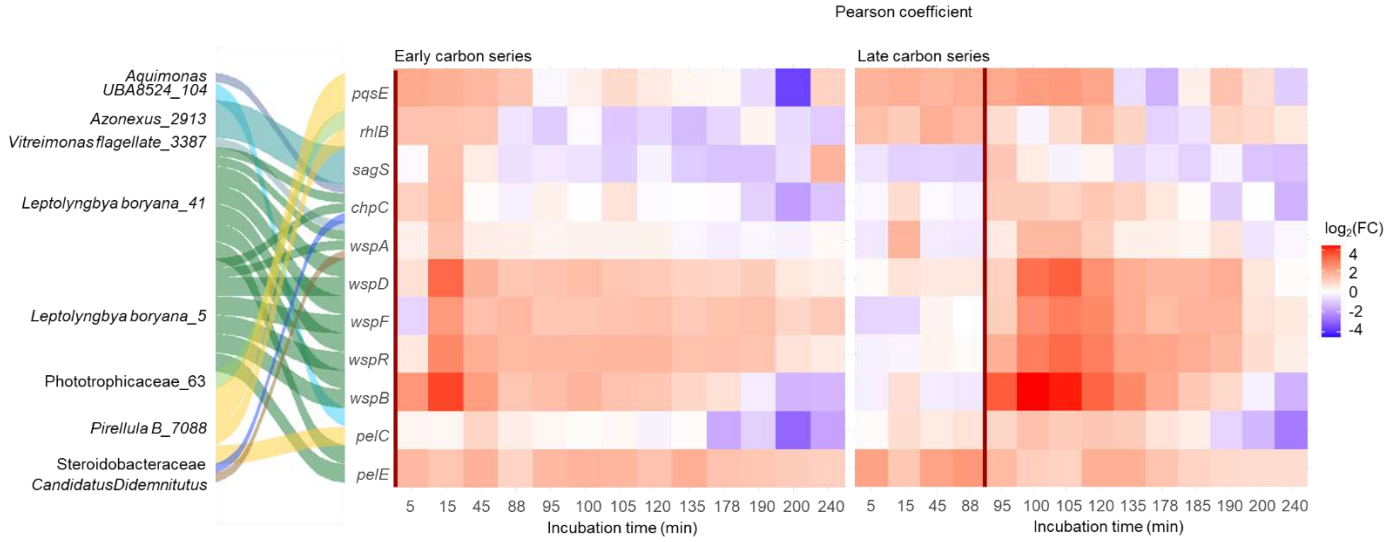
The wsp operon, found in *Leptolyngbya boryana,* is known to modulate intracellular cyclic di-GMP levels, a central second messenger governing biofilm formation, polysaccharide secretion, and surface attachment, coordinating the organization of key populations in photogranules[7,32]. Studies performed in model organisms (*Vibrio chloreae*) showed that the synergy between quorum-sensing and c-di-GMP signaling produced denser biofilms, thus enhancing community cohesion[38]. Prolonged wsp activation in the early carbon series may indicate a shift toward a more sessile state related to an increased expression of genes associated with extracellular matrix production and regulation.

Carbon history also reshaped the matrix composition. The PNAG-associated gene *icaA,* regulated by c-di-GMP[7], was active under acetate-limited conditions (late carbon series) but downregulated upon acetate addition (early carbon series, Fig. 5), whereas *pelC* activation was observed mainly in the late carbon series (Fig. 7). These different patterns suggest that acetate availability does not simply enhance EPS production but also alters its biochemical composition. Under carbon limitation, PNAG-dependent pathways contribute to EPS production and biofilm stabilization. The activation of *pelC* in the late carbon series may reflect a compensatory mechanism in response to the shorter acetate exposure, favoring structural polysaccharide production. Under sustained acetate supply, alternative polysaccharide and storage pathways (e.g., trehalose and glucans; Fig. 4) dominate, reducing reliance on pelC-mediated EPS synthesis.

In this study, acetate availability not only modulates the temporal dynamics of quorum-sensing and biofilm-regulatory gene activation but also suggests coordinated interactions between phototrophs and heterotrophs within a spatially structured consortium, involving sequential quorum-sensing signals, wsp-mediated responses, and EPS production. Through the analysis of this dynamic community, we showed that these responses are not just carbon-dependent but also carbon history-dependent, with carbon exposure time shaping both the duration and stability of regulatory activation. While cell-to-cell signaling through quorum sensing and cyclic di-GMP networks is well documented in bacterial biofilms as a mechanism for coordinating multicellular behavior and resilience[39], the temporal dynamics of these signals in response to nutrient history are less explored. In this regard, our findings provide an example of how environmental

conditions can regulate the cascade and persistence of interspecies communication events in spatially organized communities.

Fig. 7: Temporal dynamics of activated genes (log_2(Fold Change) compared to Phase 0 belonging to biofilm formation in early carbon series and late carbon series. On the left of the heatmaps, the Sankey diagram illustrates the taxa in which genes were present. The vertical brown line indicates acetate addition.



Metabolic shifts during dark phases

Switching off the light triggered a correlated metabolic shift in both early and late carbon series, towards energy conservation. Catabolic and energy-recycling pathways, including carbon and nitrogen metabolisms and aromatic compound degradation, were upregulated, whereas anabolic processes such as ribosome biogenesis, fatty acid synthesis, and starch and sucrose accumulation were downregulated (Fig. 8a-b, Tables S8-9). These metabolic shifts observed when turning off the light reversed the activation and inactivation patterns observed earlier when light was turned on (Fig. 4a, yellow sun symbols in Fig. 8a). It highlights enhanced heterotrophic activity of *Pseudogemmobacter*, *Thauera*, and members of the *Phototrophicaceae,* known for their metabolic versatility during dark/light period and aerobic/anaerobic niches[40,41]. Stored or available organic substrates supported energy generation in the absence of light. In contrast, the involvement of *Leptolyngbya boryana,* dependent of light, was more restricted, related to

porphyrin metabolism, nitrogen metabolism, and starch and sucrose pathways (Fig. 8b). None of these pathways were detected in our previous metabolomic study[12], reflecting the complementary nature of metatranscriptomic and metabolomic analysis: metatranscriptomic analysis capturing responses not necessarily observed at a metabolic level.

Prolonged acetate exposure favors metabolic and cell envelope-associated responses during dark periods

In the early carbon series, extended acetate exposure shaped a distinct response to light switch-off, activating pathways not observed in the late carbon series (Fig. 8a, red rectangles). Key processes including amino acid biosynthesis (purine, lysine, arginine), peptidoglycan biosynthesis, and lipoic acid metabolism, were activated, reflecting energy maintenance and cell-envelope remodeling.

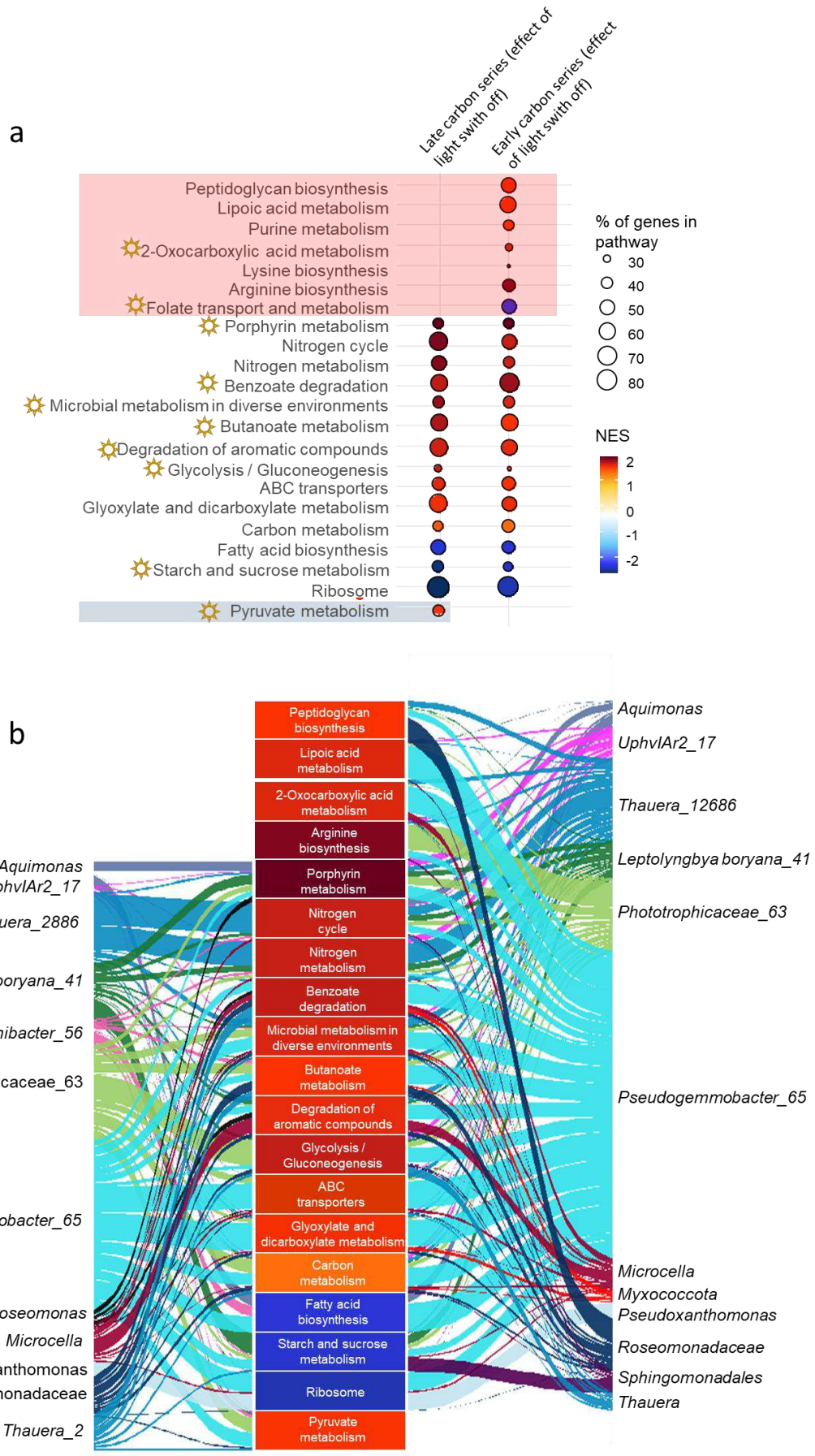
Among these pathways, arginine metabolism is particularly noteworthy due to its role in biofilm regulation: it interacts with c-di-GMP receptors, thereby modulating c-di-GMP signaling and biofilm development in bacteria and photogranules[7]. In our metabolomic study, arginosuccinate levels differed between series during phase 3 and decreased immediately after light switch-off[12], suggesting mobilization as a nitrogen-rich metabolic buffer supporting EPS production and excretion[42]. This could indicate that prolonged acetate availability allows photogranules to store amino-acids and arginine-related intermediates, enabling the community to better adapt to change in environmental conditions such as light limitation.

Peptidoglycan biosynthesis genes, including *dacB, ftsI, murA*-D*, pbp* variants, and *spo* genes, were also upregulated in the early carbon series (Table S11). These genes are involved in amino acid assembly and particularly L-alanine incorporation (Table S11). These metatranscriptomic signals align with metabolomic observation during which L-alanine was found to display different dynamics during phase 3, according to experimental series (strong increase in the early carbon series compared to a moderate increase after a lag period in the late carbon series)[12]. The activation of the peptidoglycan biosynthesis genes reflects increased cell wall biosynthetic activity that could be associated with growth and adaptation to changing environmental conditions.

Finally, lipoic acid metabolism, mainly linked to *Pseudogemmobacter* (Fig. 8b), involves central carbon and lipid-related pathways (*bkdA/B* complexes, *gcvPB, pdh, suc* genes, Table S12), promotes energy balance, membrane stability, and regulates the assembly of light-harvesting complexes under light switch-off[23,43]. Coupled with metabolomic evidence of linoleic acid remodeling during phase 3[12], these data

indicate that prolonged acetate exposure affects overall fatty acid flux and membrane composition, linking carbon history to possible changes in the cell envelope.

Fig. 8: a) KEGG pathways that were significantly enriched in the late carbon series, phase 3, or in the early carbon series, phase 3 relative to phase 2. The sun symbols indicate pathways that had the inverse response when light was switched-on. The red rectangle indicates pathways specifically enriched in the early carbon series, whereas the blue rectangle indicates pathways specifically enriched in the late carbon series. b) Sankey diagrams illustrating the contribution of the most influential contributors to the enriched KEGG pathways. Pathways are colored according to their Net Enrichment Score (NES).


a
Late carbon series (effect of light swith off)
Early carbon series (effect of light swith off)
Peptidoglycan biosynthesis
Lipoic acid metabolism
Purine metabolism
2-Oxocarboxylic acid metabolism
Lysine biosynthesis
Arginine biosynthesis
Folate transport and metabolism
Porphyrin metabolism
Nitrogen cycle
Nitrogen metabolism
Benzoate degradation
Microbial metabolism in diverse environments
Butanoate metabolism
Degradation of aromatic compounds
Glycolysis / Gluconeogenesis
ABC transporters
Glyoxylate and dicarboxylate metabolism
Carbon metabolism
Fatty acid biosynthesis
Starch and sucrose metabolism
Ribosome
Pyruvate metabolism
% of genes in pathway
30
40
50
60
70
80
NES
2
1
0
-1
-2
b
Aquimonas UphvlAr2_17
Thauera_2886
Leptolyngbya boryana_41
Phnomibacter_56
Phototrophicaceae_63
Pseudogemmobacter_65
Falsiroseomonas
Microcella
Pseudoxanthomonas
Roseomonadaceae
Thauera_2
Peptidoglycan biosynthesis
Lipoic acid metabolism
2-Oxocarboxylic acid metabolism
Arginine biosynthesis
Porphyrin metabolism
Nitrogen cycle
Nitrogen metabolism
Benzoate degradation
Microbial metabolism in diverse environments
Butanoate metabolism
Degradation of aromatic compounds
Glycolysis / Gluconeogenesis
ABC transporters
Glyoxylate and dicarboxylate metabolism
Carbon metabolism
Fatty acid biosynthesis
Starch and sucrose metabolism
Ribosome
Pyruvate metabolism
Aquimonas UphvlAr2_17
Thauera_12686
Leptolyngbya boryana_41
Phototrophicaceae_63
Pseudogemmobacter_65
Microcella
Myxococcota
Pseudoxanthomonas
Roseomonadaceae
Sphingomonadales
Thauera

393

The history of carbon supply drives, distinct metabolic responses during dark periods

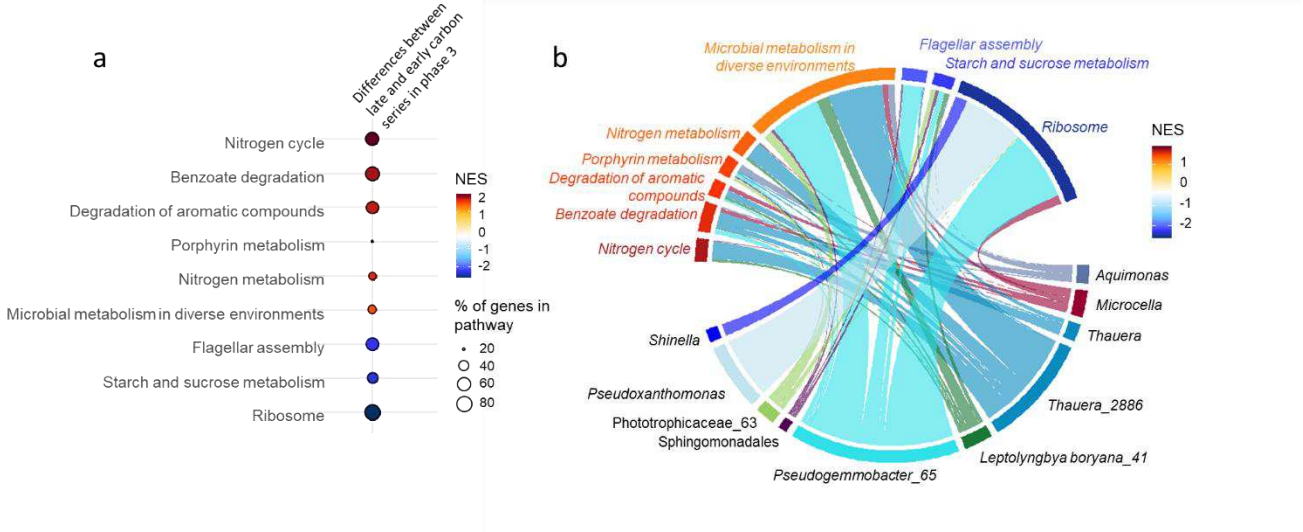
In contrast to the early carbon series, the late carbon series displayed a distinct transcriptional response when light was switched off (Fig. 9a, Table S10). Several pathways were significantly upregulated: aromatic compound degradation and nitrogen metabolism, including denitrification genes (*napA-B, nirB/S, norB-C*, *nosZ*, mainly carried by *Thauera,* Fig. 9b, Table S13) and nitrogen fixation genes (*nifD/H*, associated with *Leptolyngbya boryana* and *Azonexus*, Table S13). Darkness stopped photosynthetic oxygen production and favored denitrification[44]. When acetate was added later in the experiment, carbon remained available at the end of the light phase and served as electron donor for denitrification once the light was turned off and photosynthetic oxygen production ceased. In contrast, in the early carbon series, since available carbon had already been stored using carbohydrate pathways (Fig. 5) or acetate had been metabolized earlier, denitrification was less active.

At the same time, flagellar assembly genes (*flgC-K, flhA-B/G-N/R, hag*, *motY, rpoD*) were downregulated in the late carbon series (Fig. 9a, Table S14). In bacteria, motility is typically inversely correlated with biofilm formation[45]. Here, reduced flagellar expression correlated with the later activation of biofilm-associated genes (*wsp, sagS, chpC, pelC*), indicating a delayed transition from motile to sessile lifestyle upon light-off.

Together, these results indicate that the history of carbon addition shapes distinct dark-phase metabolic responses in photogranules. In the early carbon series, prolonged acetate exposure supports carbon storage, EPS accumulation, and cell-envelope adaptation, whereas in the late carbon series, delayed carbon availability triggers carbon and nitrogen scavenging, enhancing heterotrophic and denitrification activity. Comparison with previous metabolomic data confirms that these transcriptional patterns reflect dynamic adaptive responses, rather than being solely driven by changes in metabolite abundance, highlighting a carbon history-dependent regulation. In fluctuating environments such as wastewater treatment systems, where microbial communities are subject to variations in organic load, oxygen availability, and light exposure, carbon history can therefore influence the efficiency of nitrogen removal, probably granule cohesion and potentially affect granule stability.

Fig. 9: a) KEGG pathways that were significantly enriched in the late carbon series, phase 3, compared to the early carbon series, phase 2. b) The contributions of the most influential contributors

to the enriched KEGG pathways. Pathways are colored according to their Net Enrichment Score (NES).



Environmental conditions affect bacterial co-expression network within photogranules

Co-expression network analyses revealed that environmental conditions affected microbial interactions within photogranules at both taxonomic and topological levels (global network descriptors). At the phylum level, light availability promoted strong positive correlations between Pseudomonadota and Myxococcota, Myxococcota and Planctomycetota, Planctomycetota and Armatimonadota, as well as between Chlorobiota and Spirochaetota (Fig. S6a,b). In contrast, acetate supplementation increased negative correlations involving Cyanobacteriota and strengthened interactions between Planctomycetota and Armatimonadota (Fig. S6c,d). Delayed carbon addition further intensified negative associations with cyanobacteria, particularly with Bacteroidota, while light restoration re-established predominantly positive correlations, although network structure remained shaped by prior carbon exposure (Fig. S6e,f). These patterns suggest that light availability promotes cooperative interactions consistent with phototrophy-driven cross-feeding observed previously (Fig. 5). In contrast, acetate addition shifts the interaction network toward heterotroph-dominated processes, highlighting complementary roles in organic matter recycling and EPS-associated niches within the photogranule matrix[6,32]. The strengthening of negative associations

following delayed carbon addition may reflect a shift from cooperative phototrophy-driven interactions to competitive dynamics under direct carbon assimilation. Several of these phyla exhibited pronounced transcriptional changes despite their low abundance (Fig. 3), indicating that the restructuring of interactions paralleled an adaptation based on activity rather than community composition.

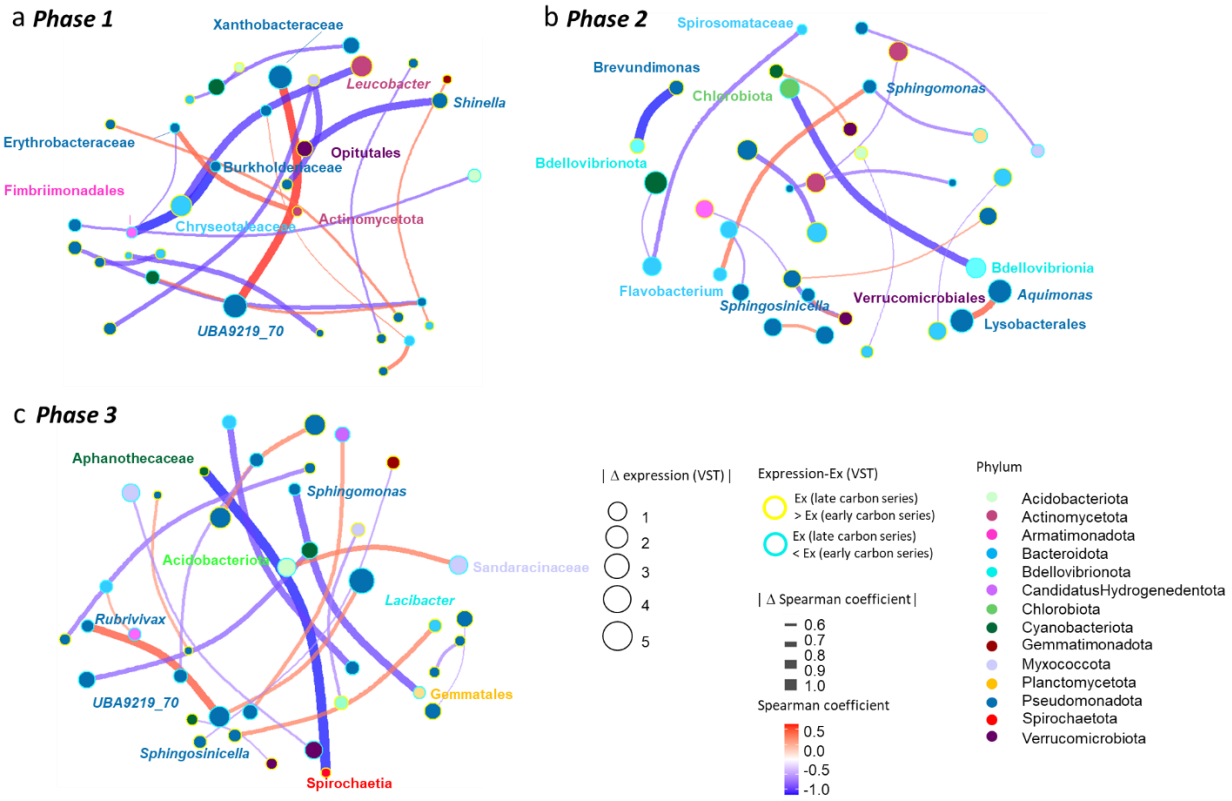
At the genus level, similar interaction patterns were observed (e.g., involving key representatives of Pseudomonadota, Planctomycetota, and Armatimonadota), supporting the consistency of these dynamics across taxonomic levels (Fig. S7). Global network descriptors clarified how carbon exposure time influenced interaction network (Table S15). Early carbon addition was associated with a network structure dominated by a limited number of highly connected taxa (higher betweenness centrality, Table S15), suggesting that specific groups rapidly respond to carbon inputs and may drive subsequent transcriptional changes in associated taxa. In contrast, delayed carbon addition led to a more evenly connected network (higher density and closeness centrality, Table S15), indicative of a more distributed response across taxa and stronger metabolic interdependence. It could explain the shorter time observed previously in biofilm formation regulatory mechanisms of the late carbon series (Fig. 7). Even during dark conditions, differences in interaction patterns persisted (closeness centrality, Table S15) showing that carbon history supply imprints interaction architecture beyond immediate environmental constraints. Such sequential and distributed transcriptional responses across multiple taxa are consistent with tightly coupled metabolic interactions, as commonly observed in syntrophic systems, where metabolic exchanges between partners constrain and coordinate their activity[46]. In this context, rapid propagation of transcriptional changes across the network likely reflects interdependencies in substrate utilization and metabolite exchange rather than independent responses to environmental change.

NetworkComparisonTest analyses[47] confirmed that each environmental transition (light shift or carbon addition) significantly affected microbial associations (Tables S16–S18, Fig. 10). Carbon availability particularly modulated interactions involving heterotrophic Pseudomonadota (Xanthobacteraceae, Erythrobacteraceae, UBA9219, *Shinella*, Burkholderiaceae) and organic matter recyclers such as Armatimonadota (Fimbriimonadales), Bacteroidota (Chryseotaleaceae), and Verrucomicrobiota (Opitutales) (Fig. 10a), while, interactions involving *Flavihumibacter* (Armatimonadota) and Planctomycetota (Pirelulaceae) or Verrucomicrobiota contributed most to network differentiation (highest global edge strength difference $E > 0.6$, Fig. S9a), consistent with the phylum-level observation made above. Delayed acetate supplementation also enhanced associations involving opportunistic or predatory taxa (e.g., Bdellovibrionota)[48] (Fig. 10b, Fig. S9b). The emergence of co-occurrence clusters including Bdellovibrionota, Chlorobiota, Flavobacteriia, and Leptolyngbyaceae (Fig.

S7) suggests intensified trophic coupling and recycling processes under fluctuating resource conditions. During dark phases, carbon history mainly affected cyanobacteria-centered interactions (between Aphanotheceae and Spirochaetia, or involving unclassified Cyanobacteriota, Fig. 10c, Fig. S8c): delayed supplementation destabilized phototroph-associated networks, whereas prolonged acetate exposure maintained stronger links between specific heterotrophic and phototrophic partners. These patterns suggest that these specific phototroph-heterotroph associations may reflect preferential trophic couplings, potentially indicative of selective syntrophic interactions within this system.

Overall, these analyses indicate that photogranule organization is governed less by dominant taxa than by highly connected populations acting as interaction hubs. Despite its high abundance, *Leptolyngbya boryana* did not emerge as a principal driver of network adaptation to environmental changes. Instead, less abundant cyanobacterial groups (e.g., Aphanotheceae and unclassified Cyanobacteriota) shaped network topology, particularly under dark conditions and delayed carbon supply, as observed in microbial dynamics where rare taxa disproportionately contribute to temporal changes in microbial diversity[18]. This finding underscores that community resilience arises from interaction reconfiguration rather than simple shifts in dominance, and that carbon history modulates not only metabolic pathways but also the identity of microbial hubs within structured consortia.

Fig. 10: Differential co-expression networks inferred from the Network Comparison Test (NCT)[47] comparing early carbon series and late carbon series in (a) phase 1, (b) phase 2, (c) phase 3. Edges represent pairwise associations that significantly differ between conditions (p value < 0.05, |E| > 0.2). Node size indicates mean change in VST expression (Δexpression), edge color shows change in Spearman correlation (Δρ), and node color corresponds to phylum. The 5 most correlated taxa are displayed here, complete names are found in Fig. S8.



A multi-omic and time-resolved framework to unravel microbial community dynamics

While it is acknowledged that deciphering microbial ecosystem functioning requires the integration of multi-omics data across time[49], implementing such approaches in dynamic and structured communities remains a major challenge. In this study, we combined metatranscriptomics and metagenomics to resolve how fast photogranule communities respond to changes in light regime and carbon availability over time. While metabolomic analyses provide direct insight into the biochemical state of the system, they may underestimate or miss key intermediates that are rapidly turned over or maintained at low concentrations. Complementing these data with metatranscriptomics therefore enables the detection of transient metabolic responses and regulatory shifts, and allows metabolite-level observations (such as the influence of carbon supplementation history on amino acid, fatty acid, or lipoic acid dynamics)[12] to be mechanistically anchored to specific pathways, genes, and taxa. Coupling these data with metagenomics further permits the

assignment of functional changes to taxonomic identities beyond dominant populations or well-resolved MAGs, revealing that transcriptional reprogramming and network restructuring are often driven by non-dominant or partially characterized taxa with specific ecological traits.

Beyond its multi-omic scope, this study adopts a longitudinal design that captures short-term temporal dynamics rarely addressed in metatranscriptomic analyses, which are often limited to comparisons between static or end-point conditions[7,9,17,32]. Our results show that community responses to light and carbon perturbations unfold through temporally structured cascades of gene expression, involving successive activation of regulatory, metabolic, and structural pathways. For instance, while cyanobacterial c-di-GMP signaling is known to coordinate biofilm formation, our time-resolved analyses reveal how this pathway is transiently modulated through quorum-sensing systems (e.g., *rhl*) and motile-to-sessile switches (e.g., *sagS*), orchestrated by distinct heterotrophic taxa such as *Pirellula* and *Azonexus*. The duration of these coordinated responses (ranging from tens of minutes to over an hour) was directly shaped by the history of carbon supplementation, highlighting the importance of temporal context in microbial regulation.

More broadly, the integrative and time-resolved framework developed here extends beyond photogranules and offers insights applicable to other syntrophic, biofilm-based systems, including wastewater treatment consortia, microbial mats, and engineered or natural phototrophic–heterotrophic aggregates. By revealing how environmental history governs not only metabolic activity but also interaction networks and regulatory hierarchies, this work contributes to a more dynamic and interaction-centered understanding of microbial community resilience and organization.

Methods

Experimental set-up

Photogranules obtained for this study were produced in a sequencing batch reactor, as described in previous papers[1,12,50]. Photogranules were then sieved to obtain biomass between 0.6 and 1 mm. From the retained biomass, 292 batches of 50 photogranules were manually selected and placed into emptied 2-mL screw-cap tubes from the FastDNA® SPIN Kit for Soil (MP Biomedicals, 6914050). For each time point, eight tubes (replicates) were immediately frozen in liquid nitrogen and stored at −70 °C. The complete procedure was already described in a previous study[12,15]. Tubes containing photogranules were exposed for 16 hours to 70 µmol·m^{-2}·s^{-1} PAR light, then kept in the dark for 3 hours to stop photosynthesis (Phase 0). The experiment began at the end of this dark period (0 min, Phase 1). In the early carbon series, 500 µL of

an aqueous solution containing 400 mg COD·L^{-1} (COD = acetate) and 21 mg NH_4^+·L^{-1} was added at 0 minutes. The same solution was added at 90 minutes in the "late carbon series." A "no-carbon series" received no external carbon or ammonium. Vials were illuminated (70 µmol·m^{-2}·s^{-1} PAR) from 0 to 180 minutes, followed by 60 minutes of darkness (Phase 3), mirroring a sequencing batch reactor cycle. Eight replicates from the early and late carbon series were sampled at 16 time points (between -2 and 240 min) while the no-carbon series was sampled at 135 and 240 minutes (Fig. 1). After sampling, tubes were immediately frozen in liquid nitrogen and stored at −80 °C until metabolite extraction. For the metatranscriptomic analysis, between 4 and 6 replicates were used, and a total of 148 samples were used for the following metatranscriptomic study. The detailled procedure can be found in another publication[12].

Metagenomic and metatranscriptomic analysis

Nucleic acid extraction

DNA for long-read metagenomic sequencing was extracted using a modified version of the FastDNA Spin Kit for Soil (MP Biomedicals, USA), as described previously[51]. RNA for metatranscriptomic sequencing was extracted using the RNeasy Mini Kit (Qiagen, catalog number: 74104), following the protocol published in BioProtocol[15].

Metagenomic and metatranscriptomic sequencing

The high-molecular-weight DNA was sequenced using PacBio Revio technology at the Gentyane INRAE platform (Clermont-Ferrand, France). A SMRTbell library was prepared using the PacBio Revio polymerase kit. Quality filtering and adapter removal were achieved automatically using SMRT Link (v.13.1.0.221970), yielding 1,814,020 HiFi reads.

Ribosomal RNA were removed from RNA extracts using the Pan-Bacteria RiboPOOL rRNA depletion kit (siTOOLs Biotech, catalog number dp-K096). The stranded paired-end libraries were prepared using Illumina stranded mRNA Prep Ligation Kit (Illumina, catalog number 20040534) and were barcoded with index adaptaters set A and set B (Illumina, catalog numbers 20091655 and 20091657). Libraries quality control was performed with Qubit (ThermoFsiher Qubit 4, DNA HS kit, catalog number Q33231) and bioanalyzer (Agilent, Bioanalyzer 2100, High Sensitivity DNA biochip, 5067-4626), their profiles were controlled using Fragment Analyzer (Agilent). The libraries (0.3 mol of each) were pooled together and the pool was subsequently sequenced on 2 lanes of an S4 flow cell on Illumina NovaSeq 6000 generating 2 × 150 bp reads, at the MGX platform (Montpellier GenomiX). The sequencer performs image analysis and

base calling in real time. Demultiplexing and the generation of FASTQ files are then carried out using the Illumina bcl-convert software.

Metagenome assembly

Metagenome assembly used in this study was described in a previous publication[51].

Metatranscriptomic analysis

Contigs obtained from long-read metagenomic assembly were taxonomically partitioned into eukaryotic and prokaryotic subsets with whokaryote v 1.1.2[52]. Structural annotation of eukaryotic contigs was performed using AUGUSTUS v 3.4.0[53] with the *Chlamydomonas reinhardtii* gene model, to take into account the presence of microalgae in photogranules, whereas prokaryotic contigs were annotated with Prodigal v 2.6.3 (default mode)[54]. Resulting annotations were reassembled using the AGAT toolkit v 1.4.1[55] and enabled the prediction of 233,578 genes (Fig. S10).

For metatranscriptomic analyses, a representative subset of 24 samples (encompassing the different conditions) was first aligned to the metagenome using the nf-core/rnaseq pipeline (v 3.18.1) with default parameters[56]. Reads were aligned with HISAT2 v 2.2.1[57], and transcript assemblies were generated with StringTie v 2.2.3[58] to refine structural annotations, resulting in the prediction of 318,083 genes. These StringTie-derived annotations were merged with the initial metagenomic annotation to produce an updated gene catalog. This catalog was then used as the reference for aligning all 148 metatranscriptomic samples, again using nf-core/rnaseq pipeline v 3.18.1 with HISAT2 v 2.2.1. Gene-level read counts were obtained with featureCounts v 2.0.6[59] using the options -M -O --fraction. Across all samples, the featureCounts assignment rate exceeded 80%, and HISAT2 alignment rates were above 70% for 97% of the samples (Fig. S11). Protein coding sequences were extracted using gffreads v 0.12.6[60], and open reading frames were predicted with TransDecoder v 5.7.1[61]. Functional annotation was performed with eggNOG-mapper v 2.1.13 [62], which yielded functional assignments for 94% of all predicted genes (Fig. S10).

The taxonomic assignments used in this study were obtained from previous analyses of metagenomic assembly and annotation[51]. If the contigs were included in the previously reported MAGs[51], taxonomic assignments were replaced by the names of the corresponding MAGs. As noted in the introduction, to specifically focus on prokaryotic interactions, and given that they accounted for over 80% of the reads throughout the experiment (Fig. S1-S2), only prokaryotic contigs were retained for the subsequent metatranscriptomic analysis.

Statistical analysis

All statistical analyses were performed in R (v 4.4.3) using the RStudio interface v 2025.9.1.401[63] Data visualizations were generated with the ggplot2 package v 3.5.1[64] unless otherwise specified in figure legends. Raw metatranscriptomic read counts were normalized using Trimmed Mean of M-values as implemented in the edgeR package v 4.4.2[65] to account for differences in sequencing depth and compositional bias among samples.

Differential expression analyses were conducted with the sanssouci package v 0.16.1[66], which provides robust control of false discoveries in high-dimensional settings. The use of sanssouci was motivated by the structure of our dataset: (i) a large number of experimental conditions (Phase 0 - Early carbon series; Phase 1 - Early carbon series; Phase 1 - Late carbon series ; Phase 2 - Early carbon series ; Phase 2 - Late carbon series ; Phase 3 - Early carbon series ; Phase 3 - Late carbon series) requiring multiple non-hierarchical pairwise comparisons; (ii) a correspondingly large number of statistical tests; (iii) potential deviations from classical parametric assumptions due to the complexity of metatranscriptomic data; and (iv) the ability of sanssouci to provide validated upper bounds on the FWER/FDR through permutation-based procedures tailored for omics-scale analyses. Pairwise differential analyses were performed for all condition contrasts.

Genes identified as significantly differentially expressed ($p < 0.05$) in each comparison were retained for functional enrichment analysis and gene expression dynamics (expressed in $\log_2$ fold change-log(FC)). Functional enrichments were computed using the clusterProfiler package v 4.16.6[67] with the KEGG database and visualized with the enrichplot R package v 1.26.6[67] and the circlize R package v 0.4.16[68]. Only pathways exhibiting significant enrichment ($p < 0.05$) were reported in the manuscript. Sankey diagrams were generated with ggalluvial v 0.12.5[69] to illustrate the contribution of the most influential contributors to the enriched KEGG pathways.

Co-occurrence networks were inferred and visualized using igraph v 2.1.4[70], and statistical comparisons of network structure were performed with the NetworkComparisonTest package v 2.2.2[47], allowing formal assessment of differences in global strength, density, and topology across conditions.

Data Availability

All sequencing data are available in the Sequence Read Archive (SRA) NCBI database under BioProject accession PRJNA1297605. The assembled metagenomic reads are deposited under the BioSample accession SAMN50229464, and the metagenome-assembled genomes (MAGs) are available

under BioSample accessions SAMN50846517 to SAMN50846541. Raw metatranscriptomic reads are available under SRA accessions from SRR36411468 to SRR36411414.

References

1. Milferstedt, K. *et al.* The importance of filamentous cyanobacteria in the development of oxygenic photogranules. *Sci Rep* **7**, 17944 (2017).
2. Billery, C., Gaval, G., Hamelin, J. & Milferstedt, K. Phototrophic aggregates for wastewater treatment: identifying key parameters for formation and characterization. *Rev Environ Sci Biotechnol* **24**, 425–450 (2025).
3. Trebuch, L. M. *et al.* High resolution functional analysis and community structure of photogranules. *The ISME Journal* **17**, 870–879 (2023).
4. Flemming, H.-C. *et al.* The biofilm matrix: multitasking in a shared space. *Nat Rev Microbiol* **21**, 70–86 (2023).
5. Brockmann, D. *et al.* Wastewater treatment using oxygenic photogranule-based process has lower environmental impact than conventional activated sludge process. *Bioresource Technology* **319**, 124204 (2021).
6. Duxbury, S. J. N. *et al.* Niche formation and metabolic interactions contribute to stable diversity in a spatially structured cyanobacterial community. *ISME J* **19**, wraf126 (2025).
7. Shi, W. *et al.* Growth progression driven by c-di-GMP in photogranules under hydrostatic conditions: polysaccharides biosynthesis and microbial interactions. *Chemical Engineering Journal* **524**, 169476 (2025).
8. Shi, J., Yang, Y., Zhu, Z., Li, S. & Zhuang, H. Enhanced efficiency of bacteria-algae symbiotic biofilm reactors in treating coal chemical wastewater: Mechanisms and microbial dynamics. *Journal of Environmental Chemical Engineering* **13**, 120096 (2025).
9. Kong, L. *et al.* Cross-Feeding between Filamentous Cyanobacteria and Symbiotic Bacteria Favors Rapid Photogranulation. *Environ. Sci. Technol.* **57**, 16953–16963 (2023).
10. Kong, L. *et al.* Interspecies hydrogen transfer between cyanobacteria and symbiotic bacteria drives nitrogen loss. *Nat Commun* **16**, 5078 (2025).
11. Cook, J. M. *et al.* Metabolome-mediated biocryomorphic evolution promotes carbon fixation in Greenlandic cryoconite holes. *Environmental Microbiology* **18**, 4674–4686 (2016).
12. Della-Negra, O. *et al.* History of carbon supply shapes the metabolic response of photogranules to light shifts. *Water Research* **281**, 123557 (2025).

13. Tong, C. *et al.* Optimizing microalgal-bacterial granular sludge performance with solar-LED nighttime light supplementation for improved wastewater treatment. *Bioresource Technology* **438**, 133197 (2025).
14. Tu, C. *et al.* Nitrogen and phosphorus preferring photogranules regulate COD/TN by carbon fixation through superposition of Chlorophyta, Cyanobacteria and Chloroflexi. *Chemical Engineering Journal* **520**, 165607 (2025).
15. Séguéla, A. *et al.* Integrated Co-extraction Protocol for Transcriptomic and ^{1}H NMR Metabolomic Analysis of Multi-species Biofilms. *BioProtocol* **15**, e5237 (2025).
16. Shen, X.-F. *et al.* The mechanism of carbon source utilization by microalgae when co-cultivated with photosynthetic bacteria. *Bioresource Technology* **365**, 128152 (2022).
17. Sato, Y. *et al.* Transcriptome analysis of activated sludge microbiomes reveals an unexpected role of minority nitrifiers in carbon metabolism. *Commun Biol* **2**, 179 (2019).
18. Shade, A. *et al.* Conditionally Rare Taxa Disproportionately Contribute to Temporal Changes in Microbial Diversity. *mBio* **5**, 10.1128/mbio.01371-14 (2014).
19. Bello, S., Howard-Azzeh, M., Schellhorn, H. E. & Gupta, R. S. Phylogenomic Analyses and Molecular Signatures Elucidating the Evolutionary Relationships amongst the Chlorobia and Ignavibacteria Species: Robust Demarcation of Two Family-Level Clades within the Order Chlorobiales and Proposal for the Family Chloroherpetonaceae fam. nov. *Microorganisms* **10**, (2022).
20. Lin, L., Chen, S., Hou, Y. & Lei, L. Study on the formation process and mechanism of aerobic granular sludge in the sequencing batch biofilter granular reactor. *Environ Sci Pollut Res* **30**, 107661–107672 (2023).
21. Weissbrodt, D. G., Neu, T. R., Kuhlicke, U., Rappaz, Y. & Holliger, C. Assessment of bacterial and structural dynamics in aerobic granular biofilms. *Front. Microbiol.* **4**, (2013).
22. Jo, J., Price-Whelan, A. & Dietrich, L. E. P. Gradients and consequences of heterogeneity in biofilms. *Nat Rev Microbiol* **20**, 593–607 (2022).
23. Abu-Ghosh, S., Dubinsky, Z., Verdelho, V. & Iluz, D. Unconventional high-value products from microalgae: A review. *Bioresource Technology* **329**, 124895 (2021).
24. Zhuang, W. *et al.* Arsenate-Induced Changes in Bacterial Metabolite and Lipid Pools during Phosphate Stress. *Applied and Environmental Microbiology* **87**, e02261-20 (2021).
25. Qian, X. *et al.* Flux balance analysis of photoautotrophic metabolism: Uncovering new biological details of subsystems involved in cyanobacterial photosynthesis. *Biochimica et Biophysica Acta (BBA) - Bioenergetics* **1858**, 276–287 (2017).

26. Pereira, S. *et al.* Complexity of cyanobacterial exopolysaccharides: composition, structures, inducing factors and putative genes involved in their biosynthesis and assembly. *FEMS Microbiol Rev* **33**, 917–941 (2009).
27. Yamborko, N. *et al.* Restoration of deuterium marker for multi-isotope mapping of cellular metabolic activity. *Sci Rep* **16**, 883 (2026).
28. Hershkovitz, N., Oren, A. & Cohen, Y. Accumulation of Trehalose and Sucrose in Cyanobacteria Exposed to Matric Water Stress. *Applied and Environmental Microbiology* **57**, 645–648 (1991).
29. Duperron, S. *et al.* Transcriptomic insights into the dominance of two phototrophs throughout the water column of a tropical hypersaline-alkaline crater lake (Dziani Dzaha, Mayotte). *Front. Microbiol.* **15**, (2024).
30. Muñoz-Marín, M. del C., López-Lozano, A., Moreno-Cabezuelo, J. Á., Díez, J. & García-Fernández, J. M. Mixotrophy in cyanobacteria. *Current Opinion in Microbiology* **78**, 102432 (2024).
31. Wolfe, A. J. The Acetate Switch. *Microbiology and Molecular Biology Reviews* **69**, 12–50 (2005).
32. Shi, Y. *et al.* Microalgal-bacterial granular sludge can remove complex organics from municipal wastewater with algae-bacteria interactions. *Commun Earth Environ* **5**, 1–10 (2024).
33. Farrow, J. M. *et al.* PqsE Functions Independently of PqsR-Pseudomonas Quinolone Signal and Enhances the rhl Quorum-Sensing System. *Journal of Bacteriology* **190**, 7043–7051 (2008).
34. Dusane, D. H. *et al.* Quorum sensing: implications on Rhamnolipid biosurfactant production. *Biotechnology and Genetic Engineering Reviews* **27**, 159–184 (2010).
35. Gupta, K., Marques, C. N. H., Petrova, O. E. & Sauer, K. Antimicrobial Tolerance of Pseudomonas aeruginosa Biofilms Is Activated during an Early Developmental Stage and Requires the Two-Component Hybrid SagS. *Journal of Bacteriology* **195**, 4975–4987 (2013).
36. Whitchurch, C. B. *et al.* Characterization of a complex chemosensory signal transduction system which controls twitching motility in Pseudomonas aeruginosa. *Molecular Microbiology* **52**, 873–893 (2004).
37. Hickman, J. W., Tifrea, D. F. & Harwood, C. S. A chemosensory system that regulates biofilm formation through modulation of cyclic diguanylate levels. *Proceedings of the National Academy of Sciences* **102**, 14422–14427 (2005).
38. Prentice, J. A., Bridges, A. A. & Bassler, B. L. Synergy between c-di-GMP and Quorum-Sensing Signaling in Vibrio cholerae Biofilm Morphogenesis. *Journal of Bacteriology* **204**, e00249-22 (2022).
39. Huang, Y., Chen, Y. & Zhang, L. The Roles of Microbial Cell-Cell Chemical Communication Systems in the Modulation of Antimicrobial Resistance. *Antibiotics* **9**, (2020).

40. Mechichi, T., Stackebrandt, E., Gad'on, N. & Fuchs, G. Phylogenetic and metabolic diversity of bacteria degrading aromatic compounds under denitrifying conditions, and description of Thauera phenylacetica sp. nov., Thauera aminoaromatica sp. nov., and Azoarcus buckelii sp. nov. *Arch Microbiol* **178**, 26–35 (2002).

41. Hanada, S. The Phylum Chloroflexi, the Family Chloroflexaceae, and the Related Phototrophic Families Oscillochloridaceae and Roseiflexaceae. in *The Prokaryotes* 515–532 (Springer, Berlin, Heidelberg, 2014). doi:10.1007/978-3-642-38954-2_165.

42. Katayama, N. & Osanai, T. Arginine inhibition of the argininosuccinate lyases is conserved among three orders in cyanobacteria. *Plant Mol Biol* **110**, 13–22 (2022).

43. Doose, C. & Hubas, C. The metabolites of light: Untargeted metabolomic approaches bring new clues to understand light-driven acclimation of intertidal mudflat biofilm. *Science of The Total Environment* **912**, 168692 (2024).

44. Yang, X. *et al.* Stabilizing photogranule systems under low-light and limited-aeration: From operational strategy to underlying mechanism. *Water Research* **289**, 125017 (2026).

45. Petrova, O. E. & Sauer, K. Sticky Situations: Key Components That Control Bacterial Surface Attachment. *Journal of Bacteriology* **194**, (2012).

46. Kouzuma, A., Kato, S. & Watanabe, K. Microbial interspecies interactions: recent findings in syntrophic consortia. *Front. Microbiol.* **6**, (2015).

47. van Borkulo, C. D. *et al.* Comparing network structures on three aspects: A permutation test. *Psychological Methods* **28**, 1273–1285 (2023).

48. Davis, S. C., Cerra, J. & Williams. Comparative genomics of obligate predatory bacteria belonging to phylum Bdellovibrionota highlights distribution and predicted functions of lineage-specific protein families. *mSphere* **9**, (2024).

49. Thakur, M. P. & Geisen, S. Trophic Regulations of the Soil Microbiome. *Trends in Microbiology* **27**, 771–780 (2019).

50. Galea-Outón, S., Milferstedt, K. & Hamelin, J. High methane potential of oxygenic photogranules decreases after starvation. *Bioresource Technology* **406**, 130986 (2024).

51. Della-Negra, O. *et al.* Metagenome-assembled genomes from oxygenic photogranules obtained from photobioreactors treating synthetic wastewater. *Microbiology Resource Announcements* **0**, e01310-25 (2026).

52. Pronk, L. J. U. & Medema, M. H. Whokaryote: distinguishing eukaryotic and prokaryotic contigs in metagenomes based on gene structure. *Microbial Genomics* **8**, 000823 (2022).

53. Stanke, M. *et al.* AUGUSTUS: ab initio prediction of alternative transcripts. *Nucleic Acids Res* **34**, W435–W439 (2006).
54. Hyatt, D. *et al.* Prodigal: prokaryotic gene recognition and translation initiation site identification. *BMC Bioinformatics* **11**, 119 (2010).
55. Dainat, J. *et al.* AGAT: Another Gff Analysis Toolkit to handle annotations in any GTF/GFF format. Zenodo https://doi.org/10.5281/zenodo.16317950 (2025).
56. Patel, H. *et al.* nf-core/rnaseq: nf-core/rnaseq v3.14.0 - Hassium Honey Badger. Zenodo https://doi.org/10.5281/zenodo.10471647 (2024).
57. Guo, J., Gao, J. & Liu, Z. HISAT2 Parallelization Method Based on Spark Cluster. *J. Phys.: Conf. Ser.* **2179**, 012038 (2022).
58. Pertea, M. *et al.* StringTie enables improved reconstruction of a transcriptome from RNA-seq reads. *Nat Biotechnol* **33**, 290–295 (2015).
59. Liao, Y., Smyth, G. K. & Shi, W. featureCounts: an efficient general purpose program for assigning sequence reads to genomic features. *Bioinformatics* **30**, 923–930 (2014).
60. Pertea, G. & Pertea, M. GFF Utilities: GffRead and GffCompare. *F1000Res* **9**, ISCB Comm J-304 (2020).
61. Haas, B. J. TransDecoder (Find Coding Regions Within Transcripts). (2025).
62. Cantalapiedra, C. P., Hernández-Plaza, A., Letunic, I., Bork, P. & Huerta-Cepas, J. eggNOG-mapper v2: Functional Annotation, Orthology Assignments, and Domain Prediction at the Metagenomic Scale. *Mol Biol Evol* **38**, 5825–5829 (2021).
63. Posit team. RStudio: Integrated Development Environment for R. Posit Software (2025).
64. Wickham, H. ggplot2. *WIREs Computational Statistics* **3**, 180–185 (2011).
65. Chen, Y., Chen, L., Lun, A. T. L., Baldoni, P. L. & Smyth, G. K. edgeR v4: powerful differential analysis of sequencing data with expanded functionality and improved support for small counts and larger datasets. *Nucleic Acids Res* **53**, gkaf018 (2025).
66. Enjalbert-Courrech, N. & Neuvial, P. Powerful and interpretable control of false discoveries in two-group differential expression studies. *Bioinformatics* **38**, 5214–5221 (2022).
67. Wu, T. *et al.* clusterProfiler 4.0: A universal enrichment tool for interpreting omics data. *Innovation* **2**, (2021).
68. Gu, Z., Gu, L., Eils, R., Schlesner, M. & Brors, B. circlize implements and enhances circular visualization in R. *Bioinformatics* **30**, 2811–2812 (2014).
69. Brunson, J. C. ggalluvial: Layered Grammar for Alluvial Plots. *Journal of Open Source Software* **5**, 2017 (2020).

70. Csárdi, G. *et al.* igraph for R: R interface of the igraph library for graph theory and network analysis. Zenodo https://doi.org/10.5281/zenodo.18637862 (2026).

Acknowledgements

This work benefited from the Environmental Biotechnology and Biorefinery Facility (Bio2E) of INRAE-LBE (doi.org/10.15454/1.557234103446854E12) for photogranule production. We thank the GeT-Biopuces platform (IBSIBA.fr https://doi.org/10.15454/08BX-VJ91, GenoToul, Toulouse, France) for performing the RNA quality control and subsequent metatranscriptomics experiments. We also thank Nathalie Vialaneix for her helpful comments on the statistical analysis of these results.

Funding Statement

This work was funded by the ANR Project Panoramics (grant number ANR-21-CE45-0036-0).

Ethics declarations

Competing interests

The authors declare no competing interests.

Supplementary Information

Supplementary Files

This is a list of supplementary files associated with this preprint. Click to download.

- 260522NatCommSIDellaNegraetal.docx
- 260522NatCommSITablesS15S18DellaNegraetal.xlsx